MATERIALS SCIENCE

Higher-order topological insulators

Frank Schindler,[1] Ashley M. Cook,[1] Maia G. Vergniory,[2,3]* Zhijun Wang,[4] Stuart S. P. Parkin,[5] B. Andrei Bernevig,[4,2,6†] Titus Neupert[1†]

Copyright © 2018 The Authors, some rights reserved; exclusive licensee American Association for the Advancement of Science. No claim to original U.S. Government Works. Distributed under a Creative Commons Attribution NonCommercial License 4.0 (CC BY-NC).

Three-dimensional topological (crystalline) insulators are materials with an insulating bulk but conducting surface states that are topologically protected by time-reversal (or spatial) symmetries. We extend the notion of three-dimensional topological insulators to systems that host no gapless surface states but exhibit topologically protected gapless hinge states. Their topological character is protected by spatiotemporal symmetries of which we present two cases: (i) Chiral higher-order topological insulators protected by the combination of time-reversal and a fourfold rotation symmetry. Their hinge states are chiral modes, and the bulk topology is $\mathbb{Z}_2$-classified. (ii) Helical higher-order topological insulators protected by time-reversal and mirror symmetries. Their hinge states come in Kramers pairs, and the bulk topology is $\mathbb{Z}$-classified. We provide the topological invariants for both cases. Furthermore, we show that SnTe as well as surface-modified Bi_2TeI, BiSe, and BiTe are helical higher-order topological insulators and propose a realistic experimental setup to detect the hinge states.

INTRODUCTION

The bulk-boundary correspondence is often taken as a defining property of topological insulators (TIs) (*1*–*3*): If a *d*-dimensional system with given symmetry is insulating in the bulk but supports gapless boundary excitations that cannot be removed by local boundary perturbations without breaking the symmetry, then the system is called TI. The electric multipole insulators in the study of Benalcazar *et al.* (*4*) generalize this bulk-boundary correspondence: In two and three dimensions, these insulators exhibit no edge or surface states, respectively, but feature gapless, topological corner excitations corresponding to quantized higher electric multipole moments. Here, we introduce a new class of three-dimensional (3D) topological phases to which the usual form of the bulk-boundary correspondence also does not apply. The topology of the bulk protects gapless states on the hinges, while the surfaces are gapped. Both systems, with gapless corner and hinge states, respectively, can be subsumed under the notion of higher-order TIs (HOTI): An *n*th-order TI has protected gapless modes at a boundary of the system of codimension *n*. Following this terminology, we introduce second-order 3D TIs in this work, while the study of Benalcazar *et al.* (*4*) has introduced second-order 2D TIs and third-order 3D TIs. The important aspect of 3D HOTIs is that they exhibit protected hinge states with (spectral) flow between the valence and conduction bands, whereas the corner states have no spectral flow.

The topological properties of HOTIs are protected by symmetries that involve spatial transformations, possibly augmented by time reversal. They thus generalize topological crystalline insulators (*5*, *6*), which have been encompassed in a recent exhaustive classification of TIs in the study of Bradlyn *et al.* (*7*). Here, we propose two cases: (i) chiral HOTIs with hinge modes that propagate unidirectionally, akin to the edge states of a 2D quantum Hall effect (*8*), or Chern insulator (*9*). We show that chiral HOTIs may be protected by the product $\hat{C}_4\hat{T}$ of time reversal $\hat{T}$ and a $\hat{C}_4$ rotation symmetry. The existence of these hinge modes—but not the direction in which they propagate—is determined by the topology of the 3D bulk. By a $\hat{C}_4\hat{T}$-respecting surface manipulation, the direction of all hinge modes can be reversed, but they cannot be removed. This constitutes a bulk $\mathbb{Z}_2$ topological classification. We also show that chiral HOTIs may have a bulk $\mathbb{Z}$ topological classification protected by mirror symmetries that leave the hinges invariant when time-reversal symmetry $\hat{T}$ is broken. (ii) helical HOTIs with Kramers pairs of counterpropagating hinge modes, akin to the edge states of a 2D quantum spin Hall effect (*1*, *10*–*12*). We show that helical HOTIs may occur when a system is invariant under time reversal $\hat{T}$ and a $\hat{C}_4$ rotation symmetry. We further show that helical HOTIs can also be protected by $\hat{T}$ and mirror symmetries that leave the hinges invariant. Any integer number of Kramers pairs is topologically protected against symmetry-preserving surface manipulations, yielding a $\mathbb{Z}$ classification.

For both cases, we show the topological bulk-surface-hinge correspondence, provide concrete lattice-model realizations, and provide expressions for the bulk topological invariants. The latter are given by the magnetoelectric polarizability and mirror Chern numbers (*6*, *13*), for chiral and helical HOTIs, respectively. For the case where a chiral HOTI also respects the product of inversion times time-reversal symmetry $\hat{I}\hat{T}$, we formulate a simplified topological index akin to the Fu-Kane formula for inversion symmetric TIs (*2*). Finally, on the basis of tight-binding and ab initio calculations, we propose SnTe as a material realization for helical HOTIs. We also propose an explicit experimental setup to cleanly create hinge states in a topological SnTe coaxial cable. In contrast, chiral HOTIs may arise in 3D TI materials that exhibit noncollinear antiferromagnetic order at low temperatures. Our work is complemented by two related articles: The study of Langbehn *et al.* (*14*) provides a general classification of second-order phases with reflection symmetry for all 10 Altland-Zirnbauer symmetry classes, and the study of Benalcazar *et al.* (*15*) establishes a physical interpretation of the topological invariants of higher-order phases in terms of electric multipole moments.

RESULTS

Chiral HOTI

We first give an intuitive argument for the topological nature of a chiral 3D HOTI. We consider a hypothetical but realizable electronic structure where gapless degrees of freedom are only found on the hinge. For

[1]Department of Physics, University of Zurich, Winterthurerstrasse 190, 8057 Zurich, Switzerland. [2]Donostia International Physics Center, P. Manuel de Lardizabal 4, 20018 Donostia–San Sebastian, Spain. [3]Department of Applied Physics II, Faculty of Science and Technology, University of the Basque Country Universidad del País Vasco, Apartado 644, 48080 Bilbao, Spain. [4]Department of Physics, Princeton University, Princeton, NJ 08544, USA. [5]Max Planck Institute of Microstructure Physics, Weinberg 2, 06120 Halle, Germany. [6]Laboratoire Pierre Aigrain, Ecole Normale Supérieure–Paris Sciences & Lettres Research University, CNRS, Université Pierre et Marie Curie–Sorbonne Universités, Université Paris Diderot–Sorbonne Paris Cité, 24 rue Lhomond, 75231 Paris Cedex 05, France.
*Present address: Ikerbasque, Basque Foundation for Science, 48013 Bilbao, Spain.
†Corresponding author. Email: titus.neupert@uzh.ch (T.N.); bernevig@princeton.edu (B.A.B.)

concreteness, let us consider a system with a square cross section, periodic boundary conditions in z direction, and $\hat{C}_4^z\hat{T}$ symmetry that has a single chiral mode at each hinge, as sketched in Fig. 1A. For these modes to be a feature associated with the 3D bulk topology of the system, they should be protected against any $\hat{C}_4^z\hat{T}$-preserving surface or hinge perturbation of the system. The minimal relevant surface perturbation of that kind is the addition of an integer quantum Hall (or Chern insulator) layer with Hall conductivity $\sigma_{xy} = e^2/h$ and $\sigma_{xy} = -e^2/h$ on the (100) surfaces and the (010) surfaces, respectively, which respects $\hat{C}_4^z\hat{T}$. As seen from Fig. 1C, this adds to each hinge two chiral hinge channels. Repeating this procedure, we can change—via a pure surface manipulation—the number of chiral channels on each hinge by any even number. Hence, only the $\mathbb{Z}_2$ parity of hinge channels can be a topological property protected by the system's 3D bulk.

A concrete model of this phase is defined via the four-band Bloch Hamiltonian

$$\mathcal{H}_c(\mathbf{k}) = \left(M + t\sum_i \cos k_i\right)\tau_z\sigma_0 + \Delta_1\sum_i \sin k_i\tau_x\sigma_i + \Delta_2(\cos k_x - \cos k_y)\tau_y\sigma_0 \quad (1)$$

where σ_i and τ_i, $i = x, y, z$, are the three Pauli matrices acting on spin and orbital degree of freedoms, respectively (see Methods for a real-space representation of the model). For $\Delta_2 = 0, \mathcal{H}_c(\mathbf{k})$ represents the well-known 3D TI if $1 < |M| < 3$. Time-reversal symmetry is represented by $T\mathcal{H}_c(\mathbf{k})T^{-1} = \mathcal{H}_c(-\mathbf{k})$, with $T \equiv \tau_0\sigma_y K$, where K denotes complex conjugation. For $\Delta_2 = 0$, Hamiltonian (1) has a $\hat{C}_4^z$ rotation symmetry $C_4^z\mathcal{H}_c(\mathbf{k})(C_4^z)^{-1} = \mathcal{H}_c(D_{\hat{C}_4^z}\mathbf{k})$, where $C_4^z \equiv \tau_0 e^{-i\frac{\pi}{4}\sigma_z}$ and $D_{\hat{C}_4^z}\mathbf{k} = (-k_y, k_x, k_z)$.

The term proportional to Δ_2 breaks both $\hat{T}$ and $\hat{C}_4^z$ individually but respects the antiunitary combination $\hat{C}_4^z\hat{T}$, which means that

$$(C_4^z T)\mathcal{H}_c(\mathbf{k})(C_4^z T)^{-1} = \mathcal{H}_c(D_{\hat{C}_4^z\hat{T}}\mathbf{k}), D_{\hat{C}_4^z\hat{T}}\mathbf{k} = (k_y, -k_x, -k_z) \quad (2)$$

is a symmetry of the Hamiltonian also when $\Delta_2 \neq 0$. Because $[\hat{C}_4^z, \hat{T}] = 0$, we have $(\hat{C}_4^z\hat{T})^4 = -1$, independent of the choice of representation.

The phase diagram of Hamiltonian (1) is shown in Fig. 2A. For $1 < |M/t| < 3$ and $\Delta_1, \Delta_2 \neq 0$, the system is a chiral 3D HOTI. The spectrum in the case of open boundary conditions in x and y directions is presented in Fig. 2C, where the chiral hinge modes (each twofold degenerate) are seen to traverse the bulk gap. Physically, the term multiplied by Δ_2 corresponds to orbital currents that break time-reversal symmetry oppositely in the x and y directions. When infinitesimally small, its main effect is thus to open gaps with alternating signs for the surface Dirac electrons of the 3D TI on the (100) and (010) surfaces. The four hinges are then domain walls at which the Dirac mass changes sign. It is well known (*16*, *17*) that such a domain wall on the surface of a 3D TI binds a gapless chiral mode, which, in the case at hand, is reinterpreted as the hinge mode of the HOTI. Another physical mechanism that breaks time-reversal symmetry and preserves $\hat{C}_4^z\hat{T}$ would be $(\pi, \pi, 0)$ noncollinear antiferromagnetic order with a unit cell as shown in Fig. 2B. Note that even with finite Δ_2, the (001) surface of the model remains gapless, because its Dirac cone is protected by the $\hat{C}_4^z\hat{T}$ symmetry that leaves the surface invariant and enforces a Kramers-like degeneracy discussed in the Supplementary Materials. The gapless nature of the (001) surface in the geometry of Fig. 1B is also required by current conservation because the chiral hinge currents cannot terminate in a gapped region of the sample. A current-conserving geometry with gapped surfaces is given in the Supplementary Materials.

We turn to the bulk topological invariant that describes the $\mathbb{Z}_2$ topology. The topological invariant of 3D TIs is the theta angle or Chern Simons invariant θ (see Methods for its definition), which is quantized by time-reversal symmetry to be $\theta = 0, \pi \bmod 2\pi$, with $\theta = \pi$ being the nontrivial case (*18*). The very same quantity θ is the topological invariant of chiral HOTIs. What changes is that its quantization to values $0, \pi$ is not enforced by $\hat{T}$ but by $\hat{C}_4\hat{T}$ symmetry in this case. θ attains a new meaning in the second-order picture: It uniquely characterizes a different symmetry-protected topological phase that exhibits $\hat{T}$-breaking but $\hat{C}_4\hat{T}$-preserving hinge currents instead of $\hat{T}$-preserving gapless surface excitations. In the Supplementary Materials, we show the quantization of θ enforced by $\hat{C}_4\hat{T}$ symmetry and explicitly evaluate $\theta = \pi$ for the model (1). We furthermore note that for a nontrivial θ in the presence of $\hat{C}_4\hat{T}$ symmetry to uniquely characterize the presence of gapless hinge excitations, the bulk and the surfaces of the material that adjoin the hinge are required to be insulating. This constitutes the bulk-surface-hinge correspondence of chiral HOTIs.

The explicit evaluation of θ is impractical for ab initio computations in generic insulators. This motivates the discussion of alternative forms of the topological invariant. The Pfaffian invariant (*1*) used to define first-order 3D TIs rests on the group relation $\hat{T}^2 = -1$, and it fails in

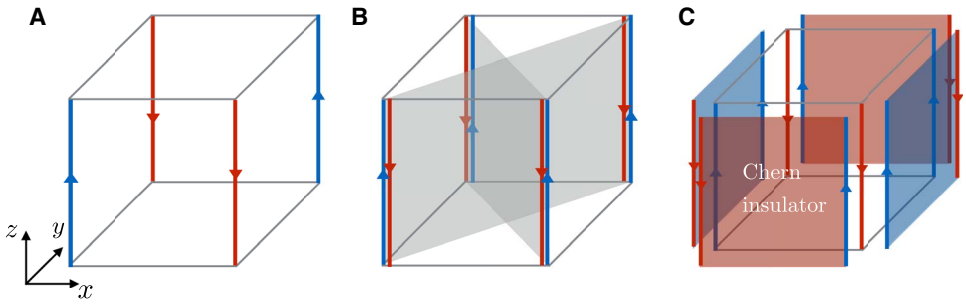

Fig. 1. Topologically protected hinge excitations of second-order 3D TIs. (**A**) Time-reversal breaking model with chiral hinge currents running along the corners of a $\hat{C}_4^z$-preserving bulk termination where periodic boundary conditions in z direction are assumed. (**B**) Time-reversal invariant model with antipropagating Kramers pairs of hinge modes. Highlighted in gray are the planes invariant under the mirror symmetries $\hat{M}_{xy}$ and $\hat{M}_{x\bar{y}}$ that protect the hinge states. (**C**) By supplementing each surface of the chiral HOTI in (A) with a Chern insulator with Hall conductivity $\sigma_{xy} = \pm e^2/h$, the number of chiral hinge modes can be changed by 2. The Hall conductivities of the additional Chern insulator layers alternate (blue for $+e^2/h$, red for $-e^2/h$) to comply with the $\hat{C}_4^z\hat{T}$ symmetry. The topology is therefore $\mathbb{Z}_2$-classified.

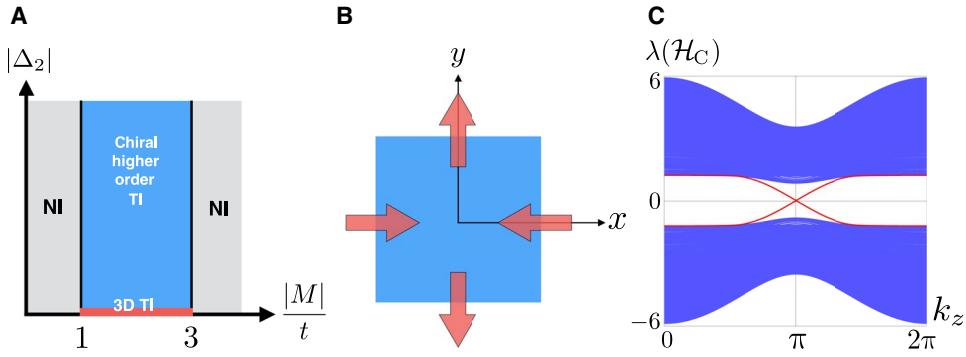

Fig. 2. Simple model for a chiral HOTI. (**A**) Schematic phase diagram for model (1), where NI stands for normal insulator. (**B**) A unit cell of noncollinear magnetic order with $\hat{C}_4^z\hat{T}$ symmetry. (**C**) Energy spectrum of model (1) with chiral hinge currents (red) in the geometry of Fig. 1A. For a slab geometry, where the bulk is terminated in just one direction of space, there are in general no gapless modes.

our case where $(\hat{C}_4\hat{T})^4 = -1$. We may instead use a non-Abelian Wilson loop characterization of the topology, as presented in the Supplementary Materials (*19*, *20*). There, we also provide two further topological characterizations, one based on so-called nested Wilson loop (*4*) and entanglement spectra (*21*–*23*) and one applicable to systems that are in addition invariant under the product $\hat{I}\hat{T}$ of inversion symmetry $\hat{I}$ and $\hat{T}$ (*3*).

Helical HOTI

Helical HOTIs feature Kramers pairs of counterpropagating hinge modes. They are protected by time-reversal symmetry and a spatial symmetry. For concreteness, let us consider a system with a square (or rhombic) cross section, periodic boundary conditions in the z direction, and two mirror symmetries $\hat{M}_{xy}$ and $\hat{M}_{x\bar{y}}$ that leave, respectively, the $x = -y$ and the $x = y$ planes invariant and with it a pair of hinges each (as sketched in Fig. 1B). We consider a hypothetical but realizable electronic structure where gapless degrees of freedom are only found on the hinge. At a given hinge, for instance, one that is invariant under $\hat{M}_{xy}$, we can choose all hinge modes as eigenstates of $\hat{M}_{xy}$. We denote the number of modes that propagate parallel, R, (antiparallel, L) to the z direction and have $\hat{M}_{xy}$ eigenvalue $i\lambda$, $\lambda = \pm 1$, by $N_{R,\lambda}$ ($N_{L,\lambda}$). We argue that the net number of helical hinge pairs $n \equiv N_{R,+} - N_{L,+}$ (which by time-reversal symmetry is equal to $N_{L,-} - N_{R,-}$) is topologically protected. In particular, n cannot be changed by any surface or hinge manipulation that respects both $\hat{T}$ and $\hat{M}_{xy}$. First, note that if both $N_{R,+}$ and $N_{L,+}$ are nonzero (assuming from now on that $N_{R,+} > N_{R,-}$), then we can always hybridize $N_{L,+}$ right-moving modes with all $N_{L,+}$ left-moving modes within the $\lambda = +$ subspace without breaking any symmetry. Therefore, only the difference n is well defined and corresponds to the number of remaining pairs of modes.

The argument for their topological protection proceeds similar to the chiral HOTI case by considering a minimal symmetry-preserving surface perturbation. It consists of a layer of a 2D time-reversal symmetric TI and its mirror-conjugated partner added to surfaces that border the hinge under consideration. Each of the TIs contributes a single Kramers pair of boundary modes to the hinge so that $(N_{L,-} + N_{L,+})$ and $(N_{R,-} + N_{R,+})$ each increase by 2 (see Fig. 3A). Because mirror symmetry maps the right-moving modes of the two Kramers pairs onto one another (and the same for the two left-moving modes), we can form a "bonding" and "antibonding" superposition with mirror eigenvalues $+i$ and $-i$ out of each pair. Thus, each of $N_{L,+}$, $N_{L,-}$, $N_{R,+}$, and $N_{R,-}$ increases by 1 because of this minimal surface manipulation. This leaves n invariant, suggesting a $\mathbb{Z}$ classification of the helical HOTI for each pair of mirror-invariant hinges. The case depicted in Fig. 1B with two mirror symmetries is then $\mathbb{Z} \times \mathbb{Z}$–classified. A more rigorous version of this argument can be found in the Supplementary Materials.

The topological invariant for the $\mathbb{Z} \times \mathbb{Z}$ classification of the helical HOTI is the set of mirror Chern numbers (*6*, *13*) $C_m/2$ on the $\hat{M}_{xy}$ and $\hat{M}_{x\bar{y}}$ mirror planes (see Methods for the definition of C_m). First, observe that if C_m were odd, then the system would be a strong 3D TI: The $\hat{M}_{xy}$ mirror planes in momentum space include all time-reversal invariant momenta in the (110) surface Brillouin zone. Thus, if C_m is odd, then there is an odd number of Dirac cones on the (110) surface, and time-reversal symmetry implies that such a system is a strong 3D TI. As the surfaces of a strong 3D TI cannot be gapped out with a time-reversal symmetric perturbation, we cannot construct a helical HOTI from it. We conclude that C_m is even for all systems of interest to us.

We now discuss the correspondence between the bulk topological invariant $C_m/2$ and the existence of Kramers-paired hinge modes. For this, we first consider the electronic structure of the (110) surface, which is invariant under $\hat{M}_{xy}$ and then that of a pair of surfaces with a normal $\mathbf{n}_\pm = (1 \pm \alpha, 1 \mp \alpha, 0)$ for small α, which are mapped into each other under $\hat{M}_{xy}$ and form a hinge at their interface (see Fig. 3, B to D).

A nonzero bulk mirror Chern number C_m with respect to the $\hat{M}_{xy}$ symmetry enforces the existence of gapless Dirac cones on the (110) surface. These Dirac cones are pinned to the mirror invariant lines $k_1 = 0, \pi$ in the surface Brillouin zone of the (110) surface, where k_1 is the momentum along the direction with the unit vector $\hat{\mathbf{e}}_1 = (\hat{\mathbf{e}}_x - \hat{\mathbf{e}}_y)/\sqrt{2}$. If we consider the electronic structure along these lines in momentum space (see Fig. 3B), then each Dirac cone has an effective Hamiltonian $\mathcal{H}_D = v_1\sigma_z(k_1 - k_1^{(0)}) + v_z\sigma_x(k_z - k_z^{(0)})$ when expanded around a Dirac point at $(k_1, k_z) = (k_1^{(0)}, k_z^{(0)})$ for $k_1^{(0)} = 0$ or $k_1^{(0)} = \pi$. The mirror symmetry is represented by $M_{xy} = i\sigma_x$, preventing mass terms of the form $m\sigma_y$ from appearing. The sign of v_z is tied to the $\hat{M}_{xy}$ eigenvalue (i sgn v_z) of the eigenstate with a positive group velocity in the z direction (at $k_1 - k_1^{(0)} = 0$). Denoting the total number of Dirac cones with $v_z > 0$ ($v_z < 0$) by n_+ (n_-), the bulk-boundary correspondence of a topological crystalline insulator (*5*) implies

$$C_m = n_+ - n_- \tag{3}$$

Consider now a pair of surfaces with slightly tilted normals $\mathbf{n}_+$ and $\mathbf{n}_-$, which are not invariant under the mirror symmetry but map into each

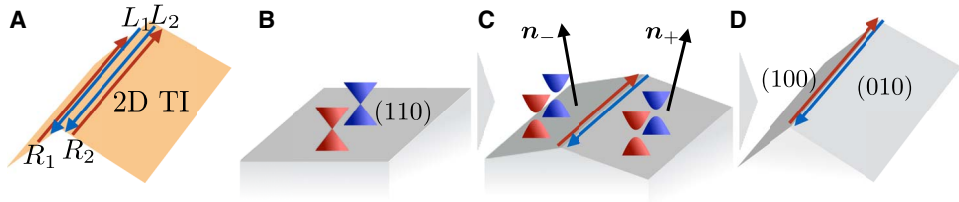

Fig. 3. Bulk-surface-hinge correspondence of helical HOTIs. (**A**) Additional hinge modes obtained by decorating the surfaces with 2D time-reversal symmetric TIs in a mirror-symmetric fashion. They can always be combined in bonding and antibonding pairs $\{R_1 + R_2, L_1 + L_2\}$ and $\{R_1 - R_2, L_1 - L_2\}$, with mirror eigenvalues $+i$ and $-i$, respectively. Therefore, they do not change the net mirror chirality of the hinge. (**B**) Mirror-symmetry protected Dirac cones on a (110) surface. (**C**) Slightly tilting the surface normal out of the mirror plane gaps the Dirac cones and forms a Kramers pair of domain wall states between two surfaces with opposite tilting. The mirror eigenvalues of the hinge modes are tied to those of the Dirac cones, which, in turn, are related to a bulk topological invariant, the mirror Chern number C_m. (**D**) Further deforming the surface to the (100) and (010) orientation in a mirror symmetry–preserving manner does not change this correspondence.

other. Mass terms are allowed, and the Hamiltonians on the surfaces with normal $\mathbf{n}_\pm$ read

$$\mathcal{H}_{D,\pm} = v_1\sigma_z\left(k_1 - k_1^{(0)} \pm \kappa\alpha\right) + v_z\sigma_x\left(k_z - k_z^{(0)}\right) \pm m\alpha\sigma_y \quad (4)$$

to linear order in α, $(k_1 - k_1^{(0)})$ and $(k_z - k_z^{(0)})$ with m and κ real parameters. The two surfaces with normals $\mathbf{n}_+$ and $\mathbf{n}_-$ meet in a hinge (see Fig. 3B). Equation 4 describes a Dirac fermion with a mass of opposite sign on the two surfaces. The hinge therefore forms a domain wall in the Dirac mass from which a single chiral channel connecting valence and conduction bands arises (*24*). As we show in the Supplementary Materials, this domain wall either binds an R moving mode with M_{xy} mirror eigenvalue $i\lambda = i\,\mathrm{sgn}(v_z)$ or an L moving mode with mirror eigenvalue $-i\,\mathrm{sgn}(v_z)$. The equality $n_{\mathrm{sgn}(v_z)} = N_{\mathrm{R,sgn}(v_z)} + N_{\mathrm{L},-\mathrm{sgn}(v_z)}$ follows, which connects the number of hinge modes $N_{\mathrm{L/R},\pm}$ we had introduced before to the mirror-graded numbers of Dirac cones on the (110) surface $\mathbf{n}_\pm$. From Eq. 3, we obtain

$$C_m = (N_{R,+} - N_{R,-} + N_{L,-} - N_{L,+}) \equiv 2n \quad (5)$$

relating the 3D bulk invariant C_m to the number of protected helical hinge pairs n of the HOTI. Notice that by time-reversal symmetry, $N_{R,+} - N_{R,-} = N_{L,-} - N_{L,+}$, so that n in Eq. 5 is an integer. C_m is even as aforementioned.

Note that the above deformation of the surfaces can be extended to nonperturbative angles α, until, for example, the (100) and (010) surface orientations are reached. The surfaces on either side of the hinge may undergo gap-closing transitions as α is increased. But as we argued at the beginning of the section, surface transitions of this kind may not change the net number of helical hinge states with a given mirror eigenvalue, if they occur in a mirror-symmetric manner.

We remark that an equation similar to Eq. 5 also holds in the absence of time-reversal symmetry for each mirror subspace. Then, the Chern number in each mirror subspace is an independent topological invariant, which gives rise to a $\mathbb{Z} \times \mathbb{Z}$ classification on each hinge (as opposed to $\mathbb{Z}$ with time-reversal symmetry). This case corresponds to chiral HOTIs protected by mirror symmetries instead of the $\hat{C}_4\hat{T}$ symmetry used in Eq. 2. Conversely, we show in the Supplementary Materials that a helical HOTI protected by $\hat{C}_4$ and $\hat{T}$ exists and has a $\mathbb{Z}_2$ classification.

Material candidates and experimental setup

We propose that SnTe realizes a helical HOTI. In its cubic rocksalt structure, SnTe is known to be a topological crystalline insulator (*5*, *6*). This crystal structure has mirror symmetries $\hat{M}_{xy}$ [acting as $(x, y, z) \rightarrow (y, x, z)$] as well as its partners under cubic symmetry ($\hat{M}_{x\bar{y}}$, $\hat{M}_{xz}$, $\hat{M}_{x\bar{z}}$, $\hat{M}_{yz}$, and $\hat{M}_{y\bar{z}}$). Further spatial symmetries irrelevant to the discussion are not mentioned. The bulk electronic structure of SnTe is insulating and topologically characterized by a mirror Chern number $C_m = 2$ with respect to the mirror symmetries on the mirror planes that include the Γ point in momentum space. All other mirror planes have $C_m = 0$. As a result, cubic SnTe has mirror-symmetry protected Dirac cones on specific surfaces. We consider the geometry of Fig. 1B with open boundary conditions in the x and y directions and periodic boundary conditions in the z direction. The $\hat{M}_{xz}$, $\hat{M}_{x\bar{z}}$, $\hat{M}_{yz}$, and $\hat{M}_{y\bar{z}}$ symmetries along with their mirror Chern numbers protect either four Dirac cones at generic surface momenta or two at the surface Brillouin zone Kramers points on the (100) as well as the (010) surfaces (see Fig. 4B). In the case at hand, the former possibility is realized. We now discuss two distortions of the crystal structure that turn SnTe into a HOTI.

(1) At about 98 K, SnTe undergoes a structural distortion into a low-temperature rhombohedral phase via a relative displacement of the two sublattices along the (111) direction (*25*, *26*). This breaks the mirror symmetries $\hat{M}_{x\bar{z}}$, $\hat{M}_{y\bar{z}}$, and $\hat{M}_{x\bar{y}}$ but preserves $\hat{M}_{xz}$, $\hat{M}_{yz}$, and $\hat{M}_{xy}$. On the (100) surface in the geometry in Fig. 1B, for instance, the two Dirac cones protected by $\hat{M}_{y\bar{z}}$ can thus be gapped out, while the two Dirac cones protected by $\hat{M}_{yz}$ remain [and similarly for the (010) surface]. Therefore, the (100) and (010) surfaces remain gapless, and the geometry of Fig. 1B cannot be used to expose the HOTI nature of SnTe with (111) uniaxial displacement. For that reason, we instead consider the $(\bar{1}01)$ and $(0\bar{1}1)$ surfaces, which are not invariant under any mirror symmetry of SnTe with (111) uniaxial displacement. The spectral function focused on the hinge weight of a semi-infinite geometry with a single hinge formed between the $(\bar{1}01)$ and $(0\bar{1}1)$ surfaces is shown in Fig. 4E. This tight-binding calculation, based on density functional theory (DFT)–derived Wannier functions (WFs) (see Methods), demonstrates the existence of this single Kramers pair of states on the two hinges invariant under $\hat{M}_{xy}$, in line with the prediction of Eq. 5 for $C_m = 2$.

(2) If uniaxial strain along the (110) direction is applied to SnTe, then $\hat{M}_{xz}$, $\hat{M}_{x\bar{z}}$, $\hat{M}_{yz}$, and $\hat{M}_{y\bar{z}}$ symmetries are broken, but $\hat{M}_{xy}$ and $\hat{M}_{x\bar{y}}$ are preserved. This gaps the (100) and (010) surfaces in the geometry in Fig. 1B completely. We calculated the surface states by using a slab geometry along the (100) direction with DFT. Because of the smallness of the bandgap induced by strain, we needed to achieve a negligible

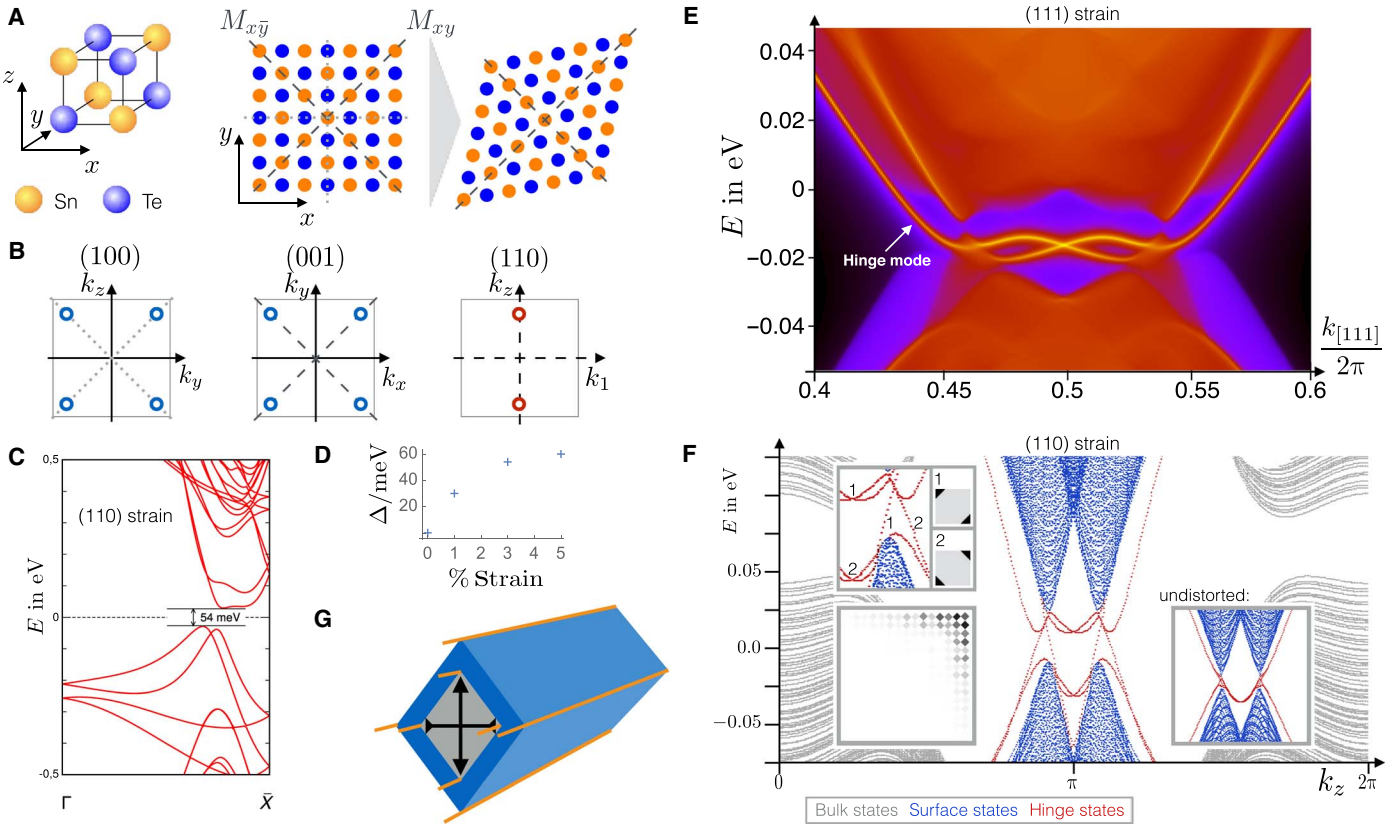

Fig. 4. Helical HOTI emerging from the topological crystalline insulator SnTe. (**A**) Rocksalt lattice structure of SnTe. Uniaxial strain along the (110) direction breaks the mirror symmetries represented by dotted lines but preserves the ones represented by dashed lines. (**B**) Circles indicate the location of Dirac cones in the surface Brillouin zone of pristine SnTe for various surface terminations. Those crossed by dotted mirror symmetries are gapped in SnTe with uniaxial strain while the others are retained. The two red Dirac cones are enforced by a mirror Chern number $C_m = 2$, corresponding to one helical pair of hinge modes. k_1 is the momentum along the direction with unit vector $\hat{\mathbf{e}}_1 = (\hat{\mathbf{e}}_x - \hat{\mathbf{e}}_y)/\sqrt{2}$. (**C**) DFT band structure of a slab of SnTe with open boundary conditions in the (100) direction under 3% strain in the (110) direction. (**D**) DFT calculation of the gap Δ that develops on the (100) surface of SnTe under (110) uniaxial strain. (**E**) DFT-based Wannier tight-binding calculation of SnTe with the (111) ferroelectric displacement in a semi-infinite geometry in which the $(0\bar{1}1)$ surface and the $(\bar{1}01)$ surface meet at a hinge that is parallel to the (111) direction. A single Kramers pair of hinge states is visible. This distortion breaks all mirror symmetries except those with normal $(0\bar{1}1)$, $(\bar{1}01)$, and $(1\bar{1}0)$, which retain their mirror Chern number 2 for a sufficiently small distortion. The $(0\bar{1}1)$ and $(\bar{1}01)$ surfaces considered here are both not invariant under these mirror symmetries, but the hinge formed between them is invariant under the mirror symmetry with normal $(1\bar{1}0)$, supporting topological hinge states. (**F**) Low-energy finite size spectrum of SnTe with uniaxial (110) strain obtained using a tight-binding model (see the Supplementary Materials) for open boundary conditions in the *x* and *y* directions (with $L_x = L_y = 111$ atoms) and periodic boundary conditions in the *z* direction. States localized in the bulk, on the (100)/(010) surfaces, and on the hinges are color-coded. Near $k_z = \pi$, four Kramers pairs of hinge modes, one localized on each hinge, are found. Upper left inset: Localization of the gapless modes. Lower left inset: Spatial structure of one such mode near a hinge. Only a small portion of the lattice near the hinge is shown. Right inset: Electronic structure of undistorted SnTe in the same geometry, showing two "flat band" hinge modes in addition to the gapless surface Dirac cones. (**G**) Topological coaxial cable geometry to realize (110) uniaxial displacement. A Si or SiO substrate (gray) is etched to have a rhombohedral cross section and then coated with SnTe (blue) yielding Kramers pairs of hinge modes (orange).

interaction between the surface states from both sides of the slab. To reduce the overlap between top and bottom surface states, we considered a slab of 45 layers and 1 nm vacuum thickness, artificially localized the states on one of the surfaces, and added one layer of hydrogen on one of the surfaces. The evolution of the surface gap size with strain is shown in Fig. 4D (see the Supplementary Materials for more details). Figure 4F is the spectrum of a tight-binding calculation (*6*) with (110) strain, demonstrating that there exists one Kramers pair of hinge modes on all four hinges in the geometry of Fig. 1B.

We propose to physically realize the (110) uniaxial strain in SnTe with a topological coaxial cable geometry, which would enable the use of its protected hinge states as quasi-1D dissipationless conduction channels (see Fig. 4F). The starting point is an insulating nanowire substrate made from Si or SiO, with a slightly rhombohedral cross section imprinted by anisotropic etching. SnTe is grown in layers on the surfaces by using molecular beam epitaxy, with a thickness of about 10 layers. SnTe will experience the uniaxial strain to gap out its surfaces and protect the helical HOTI phase. The hinge states can be studied by scanning tunneling microscopy and transport experiments with contacts applied through electronic-beam lithography. Note that in the process of growth, regions with step edges are likely to form on the surfaces and should be avoided in measurements, as they may carry their own gapless modes (*27*). Alternatively, we propose to use a superconducting substrate to study proximity-induced superconductivity on the helical hinge states.

In addition to the topological crystalline insulator SnTe, we propose weak TIs with nonvanishing mirror Chern numbers as possible avenues to realize helical HOTIs. We computed the relevant mirror Chern numbers for the weak TIs Bi_2TeI (*28*), BiSe (*29*), and BiTe (*30*), which all turn out to be 2. These materials are therefore dual TIs, in the sense

that they carry nontrivial weak and crystalline topological invariants. Their surface Dirac cones are protected by a nontrivial weak index, that is, by time reversal together with translation symmetry. To gap them, it is necessary to break at least one of these symmetries, which is possible by inducing magnetic or charge density wave order.

DISCUSSION

We have introduced 3D HOTIs, which have gapped surfaces but gapless hinge modes, as intrinsically 3D topological phases of matter. Both time-reversal symmetry breaking and time-reversal symmetric systems were explored, which support hinge states akin to those of the integer quantum Hall effect and 2D time-reversal symmetric TIs, respectively. The former may be realized in magnetically ordered TIs; we propose the naturally occurring rhombohedral or a uniaxially distorted phase of SnTe as a material realization for the latter. Despite their global topological characterization based on spatial symmetries, the hinge states are as robust against local perturbations as quantum (spin) Hall edge modes. The concepts introduced here can be extended to define novel topological superconductors with chiral and helical Majorana modes at their hinges and may further be transferred to strongly interacting, possibly topologically ordered, states of matter and to mechanical (*31*), electrical (*32*), and photonic analogs of Bloch Hamiltonians.

METHODS

First-principles calculations

We used DFT as implemented in the Vienna Ab initio Simulation Package (*33*). The exchange correlation term was described according to the Perdew-Burke-Ernzerhof prescription together with projected augmented-wave pseudopotentials (*34*). For the autoconsistent calculations, we used a 12 × 12 × 12 **k**-point mesh for the bulk and 7 × 7 × 1 for the slab calculations.

For the electronic structure of SnTe with (110) distortion, the kinetic energy cutoff was set to 400 eV. We calculated the surface states by using a slab geometry along the (100) direction. Because of the smallness of the bandgap induced by strain, we needed to achieve a negligible interaction between the surface states from both sides of the slab (to avoid a spurious gap opened by the creation of bonding and antibonding states from the top and bottom surface states). To reduce the overlap between top and bottom surface states, we considered a slab of 45 layers and 1 nm vacuum thickness and artificially localized the states on one of the surfaces. The latter was performed by adding one layer of hydrogen to one of the surfaces.

To obtain the electronic structure of bulk SnTe with (111) ferroelectric distortion, we set the cutoff energy for wave-function expansion to 500 eV. We used the parameter λ introduced in the study of Plekhanov *et al.* (*35*) to parameterize a path linearly connecting the cubic structure (space group *Fm*3*m*) to the rhombohedral structure (space group *R*3*m*). Our calculations are focused on the λ = 0.1 structure. Then, to obtain the hinge electronic structure, we first constructed the maximally localized WFs from the bulk ab initio calculations. These WFs were used in a Green's function calculation for a system finite in *a* direction, semi-infinite in *b* direction, and periodic in *c* direction (*a*, *b*, and *c* are the conventional lattice vectors in the space group *R*3*m*). The hinge state spectrum was obtained by projecting on the atoms at the corner, which preserve the mirror symmetry $\hat{M}_{xy}$.

Chiral HOTI tight-binding model

We considered a model on a simple cubic lattice spanned by the basis vectors $\hat{\mathbf{e}}_i$, $i = x, y, z$, with two orbitals $d_{x^2-y^2}$ (denoted α = 0 below) and $f_{z(x^2-y^2)}$ (α = 1) on each site, which is populated by spin $^1/_2$ electrons. It is defined by the tight-binding Hamiltonian

$$\begin{aligned} H_c = & \frac{M}{2}\sum_{\mathbf{r},\alpha}(-1)^{\alpha} c^{\dagger}_{\mathbf{r},\alpha} c_{\mathbf{r},\alpha} \\ & + \frac{t}{2}\sum_{\mathbf{r},\alpha}\sum_{i=x,y,z}(-1)^{\alpha}\, c^{\dagger}_{\mathbf{r}+\hat{\mathbf{e}}_i,\alpha} c_{\mathbf{r},\alpha} \\ & + \frac{\Delta_1}{2}\sum_{\mathbf{r},\alpha}\sum_{i=x,y,z} c^{\dagger}_{\mathbf{r}+\hat{\mathbf{e}}_i,\alpha+1}\sigma_i c_{\mathbf{r},\alpha} \\ & - \frac{\Delta_2}{2i}\sum_{\mathbf{r},\alpha}\sum_{i=x,y,z}(-1)^{\alpha} n_i c^{\dagger}_{\mathbf{r}+\hat{\mathbf{e}}_i,\alpha+1} c_{\mathbf{r},\alpha} + \text{h.c.} \end{aligned} \tag{6}$$

where α is defined modulo 2, $\hat{\mathbf{n}} = (1, -1, 0)$, and $c^{\dagger}_{\mathbf{r},\alpha} = (c^{\dagger}_{\mathbf{r},\alpha,\uparrow} c^{\dagger}_{\mathbf{r},\alpha,\downarrow})$ creates a spinor in orbital α at lattice site **r**. We denoted by σ_0 and σ_i, $i = x, y, z$, respectively, the 2 × 2 identity matrix and the three Pauli matrices acting on the spin $^1/_2$ degree of freedom.

Chern-Simons topological invariant

The invariant for chiral HOTIs with $\hat{C}_4\hat{T}$ symmetry is given by

$$\theta = \frac{1}{4\pi}\int d^3\mathbf{k}\epsilon_{abc}\mathrm{tr}\left[\mathcal{A}_a\partial_b\mathcal{A}_c + i\frac{2}{3}\mathcal{A}_a\mathcal{A}_b\mathcal{A}_c\right] \tag{7}$$

written in terms of the Berry gauge field $\mathcal{A}_{a;n,n'} = -i\langle u_n|\partial_a|u_{n'}\rangle$, where $|u_n\rangle$ are the Bloch eigenstates of the Bloch Hamiltonian and n, n' are running over the occupied bands of the insulator. ∂_a is the partial derivative with respect to the momentum component k_a, $a = x, z, y$. The trace is performed with respect to band indices.

Mirror Chern number

The topological invariant of a 3D helical HOTI is the mirror Chern number C_m. Because for a spinful system a mirror symmetry $\hat{M}$ satisfies $\hat{M}^2 = -1$, its representation M has eigenvalues ± i. Given a surface Σ in the Brillouin zone, which is left invariant under the action of $\hat{M}$, the eigenstates $|u_n\rangle$ of the Bloch Hamiltonian on Σ can be decomposed into two groups, $\{|u_l^+\rangle\}$ and $\{|u_l^-\rangle\}$, with mirror eigenvalue ±i, respectively. Time-reversal symmetry maps one mirror eigenspace into the other; if time-reversal symmetry is present, then the two mirror eigenspaces are of the same dimension. We can define the Chern number in each mirror subspace as

$$C_{\pm} = \frac{1}{2\pi}\int_{\Sigma} dk_x dk_y \mathcal{F}^{\pm}_{xy}(\mathbf{k}) \tag{8}$$

Here

$$\mathcal{F}^{\pm}_{ab}(\mathbf{k}) = \partial_a\mathcal{A}^{+}_b(\mathbf{k}) - \partial_b\mathcal{A}^{+}_a(\mathbf{k}) + i\left[\mathcal{A}^{+}_a(\mathbf{k}), \mathcal{A}^{+}_b(\mathbf{k})\right] \tag{9}$$

is the non-Abelian Berry curvature field in the $\pm i$ mirror subspace, with $\mathcal{A}^{\pm}_{a;l,l'} = -i\langle u^{\pm}_{l}|\partial_a|u^{\pm}_{l'}\rangle$, and matrix multiplication is implied in the expressions. Note that in time-reversal symmetric systems, $C_+ = -C_-$, and we define the mirror Chern number

$$C_{\mathrm{m}} \equiv (C_+ - C_-)/2 \tag{10}$$

SUPPLEMENTARY MATERIALS

Supplementary material for this article is available at http://advances.sciencemag.org/cgi/content/full/4/6/eaat0346/DC1

Supplementary Text

fig. S1. Nested entanglement and Wilson loop spectra for the second-order 3D chiral TI model defined in Eq. 1 in the main text with $M/t = 2$ and $\Delta_1/t = \Delta_2/t = 1$.

fig. S2. Real-space hopping picture for the optical lattice model with $H_4 = \sum_{\langle ij\rangle\in(x,y)}\left(t^{(x,y)}_{ij}c^{\dagger}_{z,i}c_{z,j} + t^{z}_{ij}c^{\dagger}_{z,i}c_{z+1,j}\right)$.

fig. S3. Real-space structure for a chiral HOTI.

fig. S4. Constraints on mirror-symmetric domain wall modes in two dimensions.

fig. S5. Wilson loop characterization of helical HOTIs.

fig. S6. Band structure of the surface Dirac cones of the topological crystalline insulator SnTe calculated in a slab geometry.

fig. S7. High-symmetry points in the BZ of SnTe.

References (*36–40*)

REFERENCES AND NOTES

1. C. L. Kane, E. J. Mele, Z_2 topological order and the quantum spin Hall effect. *Phys. Rev. Lett.* **95**, 146802 (2005).
2. L. Fu, C. L. Kane, E. J. Mele, Topological insulators in three dimensions. *Phys. Rev. Lett.* **98**, 106803 (2007).
3. L. Fu, C. L. Kane, Topological insulators with inversion symmetry. *Phys. Rev. B* **76**, 045302 (2007).
4. W. A. Benalcazar, B. A. Bernevig, T. L. Hughes, Quantized electric multipole insulators. *Science* **357**, 61–66 (2017).
5. L. Fu, Topological crystalline insulators. *Phys. Rev. Lett.* **106**, 106802 (2011).
6. T. H. Hsieh, H. Lin, J. Liu, W. Duan, A. Bansil, L. Fu, Topological crystalline insulators in the SnTe material class. *Nat. Commun.* **3**, 982 (2012).
7. B. Bradlyn, L. Elcoro, J. Cano, M. G. Vergniory, Z. Wang, C. Felser, M. I. Aroyo, B. A. Bernevig, Topological quantum chemistry. *Nature* **547**, 298–305 (2017).
8. K. v. Klitzing, G. Dorda, M. Pepper, New method for high-accuracy determination of the fine-structure constant based on quantized Hall resistance. *Phys. Rev. Lett.* **45**, 494 (1980).
9. F. D. M. Haldane, Model for a quantum Hall effect without Landau levels: Condensed-matter realization of the "parity anomaly". *Phys. Rev. Lett.* **61**, 2015–2018 (1988).
10. X.-L. Qi, Y.-S. Wu, S.-C. Zhang, Topological quantization of the spin Hall effect in two-dimensional paramagnetic semiconductors. *Phys. Rev. B* **74**, 085308 (2006).
11. B. A. Bernevig, T. L. Hughes, S.-C. Zhang, Quantum spin Hall effect and topological phase transition in HgTe quantum wells. *Science* **314**, 1757–1761 (2006).
12. B. A. Bernevig, S.-C. Zhang, Quantum spin Hall effect. *Phys. Rev. Lett.* **96**, 106802 (2006).
13. J. C. Y. Teo, L. Fu, C. L. Kane, Surface states and topological invariants in three-dimensional topological insulators: Application to $Bi_{1-x}Sb_x$. *Phys. Rev. B* **78**, 045426 (2008).
14. J. Langbehn, Y. Peng, L. Trifunovic, F. von Oppen, P. W. Brouwer, Reflection-symmetric second-order topological insulators and superconductors. *Phys. Rev. Lett.* **119**, 246401 (2017).
15. W. A. Benalcazar, B. A. Bernevig, T. L. Hughes, Electric multipole moments, topological multipole moment pumping, and chiral hinge states in crystalline insulators. *Phys. Rev. B* **96**, 245115 (2017).
16. M. Sitte, A. Rosch, E. Altman, L. Fritz, Topological insulators in magnetic fields: Quantum Hall effect and edge channels with a nonquantized θ term. *Phys. Rev. Lett.* **108**, 126807 (2012).
17. F. Zhang, C. L. Kane, E. J. Mele, Surface state magnetization and chiral edge states on topological insulators. *Phys. Rev. Lett.* **110**, 046404 (2013).
18. X.-L. Qi, T. L. Hughes, S.-C. Zhang, Topological field theory of time-reversal invariant insulators. *Phys. Rev. B* **78**, 195424 (2008).
19. R. Yu, X. L. Qi, A. Bernevig, Z. Fang, X. Dai, Equivalent expression of $\mathbb{Z}_2$ topological invariant for band insulators using the non-Abelian Berry connection. *Phys. Rev. B* **84**, 075119 (2011).
20. A. Alexandradinata, X. Dai, B. A. Bernevig, Wilson-loop characterization of inversion-symmetric topological insulators. *Phys. Rev. B* **89**, 155114 (2014).
21. H. Li, F. D. M. Haldane, Entanglement spectrum as a generalization of entanglement entropy: Identification of topological order in non-Abelian fractional quantum Hall effect states. *Phys. Rev. Lett.* **101**, 010504 (2008).
22. I. Peschel, Calculation of reduced density matrices from correlation functions. *J. Phys. A Math. Gen.* **36**, L205 (2003).
23. L. Fidkowski, Entanglement spectrum of topological insulators and superconductors. *Phys. Rev. Lett.* **104**, 130502 (2010).
24. R. Jackiw, C. Rebbi, Solitons with fermion number ½. *Phys. Rev. D* **13**, 3398 (1976).
25. M. Iizumi, Y. Hamaguchi, K. F. Komatsubara, Y. Kato, Phase transition in SnTe with low carrier concentration. *J. Phys. Soc. Jpn.* **38**, 443–449 (1975).
26. T. Liang, S. Kushwaha, J. Kim, Q. Gibson, J. Lin, N. Kioussis, R. J. Cava, N. P. Ong, A pressure-induced topological phase with large Berry curvature in $Pb_{1-x}Sn_xTe$. *Sci. Adv.* **3**, e1602510 (2017).
27. P. Sessi, D. Di Sante, A. Szczerbakow, F. Glott, S. Wilfert, H. Schmidt, T. Bathon, P. Dziawa, M. Greiter, T. Neupert, G. Sangiovanni, T. Story, R. Thomale, M. Bode, Robust spin-polarized midgap states at step edges of topological crystalline insulators. *Science* **354**, 1269–1273 (2016).
28. I. P. Rusinov, T. V. Menshchikova, A. Isaeva, S. V. Eremeev, Y. M. Koroteev, M. G. Vergniory, P. M. Echenique, E. V. Chulkov, Mirror-symmetry protected non-TRIM surface state in the weak topological insulator Bi_2TeI. *Sci. Rep.* **6**, 20734 (2016).
29. K. Majhi, K. Pal, H. Lohani, A. Banerjee, P. Mishra, A. K. Yadav, R. Ganesan, B. R. Sekhar, U. V. Waghmare, P. S. A. Kumar, Emergence of a weak topological insulator from the Bi_xSe_y family. *Appl. Phys. Lett.* **110**, 162102 (2017).
30. M. Eschbach, M. Lanius, C. Niu, E. Młyńczak, P. Gospodarič, J. Kellner, P. Schüffelgen, M. Gehlmann, S. Döring, E. Neumann, M. Luysberg, G. Mussler, L. Plucinski, M. Morgenstern, D. Grützmacher, G. Bihlmayer, S. Blügel, C. M. Schneider, Bi_1Te_1 is a dual topological insulator. *Nat. Commun.* **8**, 14976 (2017).
31. M. Serra-Garcia, V. Peri, R. Süsstrunk, O. R. Bilal, T. Larsen, L. G. Villanueva, S. D. Huber, Observation of a phononic quadrupole topological insulator. *Nature* **555**, 342–345 (2018).
32. S. Imhof, C. Berger, F. Bayer, J. Brehm, L. Molenkamp, T. Kiessling, F. Schindler, C. H. Lee, M. Greiter, T. Neupert, R. Thomale, Topolectrical circuit realization of topological corner modes. arXiv:1708.03647 (2017).
33. G. Kresse, J. Furthmüeller, Efficiency of ab-initio total energy calculations for metals and semiconductors using a plane-wave basis set. *Comput. Mater. Sci.* **6**, 15–50 (1996).
34. J. P. Perdew, K. Burke, M. Ernzerhof, Generalized gradient approximation made simple. *Phys. Rev. Lett.* **77**, 3865–3868 (1996).
35. E. Plekhanov, P. Barone, D. Di Sante, S. Picozzi, Engineering relativistic effects in ferroelectric SnTe. *Phys. Rev. B* **90**, 161108 (2014).
36. J.-P. Hanke, F. Freimuth, S. Blügel, Y. Mokrousov, Prototypical topological orbital ferromagnet γ-FeMn. *Sci. Rep.* **7**, 41078 (2017).
37. I. C. Fulga, N. Avraham, H. Beidenkopf, A. Stern, Coupled-layer description of topological crystalline insulators. *Phys. Rev. B* **94**, 125405 (2016).
38. J. Liu, W. Duan, L. Fu, Two types of surface states in topological crystalline insulators. *Phys. Rev. B* **88**, 241303 (2013).
39. Y. J. Wang, W.-F. Tsai, H. Lin, S.-Y. Xu, M. Neupane, M. Z. Hasan, A. Bansil, Nontrivial spin texture of the coaxial Dirac cones on the surface of topological crystalline insulator SnTe. *Phys. Rev. B* **87**, 235317 (2013).
40. R. Jackiw, P. Rossi, Zero modes of the vortex-fermion system. *Nucl. Phys. B* **190**, 681–691 (1981).

Acknowledgments: B.A.B. wishes to thank Ecole Normale Superieure, Université Pierre et Marie Curie, Paris, and Donostia International Physics Center for their sabbatical hosting during some of the stages of this work. **Funding:** F.S. and T.N. acknowledge support from the Swiss National Science Foundation (grant number: 200021_169061) and from the European Union's Horizon 2020 research and innovation program (ERC-StG-Neupert-757867-PARATOP). A.M.C. wishes to thank the Aspen Center for Physics, which is supported by NSF grant PHY-1066293, for hosting during some stages of this work. M.G.V. was supported by FIS2016-75862-P national projects of the Spanish Ministry of Economy and Competitiveness. B.A.B. acknowledges support for the analytic work from the Department of Energy (de-sc0016239), Simons Investigator Award, the Packard Foundation, and the Schmidt Fund for Innovative Research. The computational part of the Princeton work was performed under NSF Early-Concept Grants for Exploratory Research grant DMR-1643312, ONR-N00014-14-1-0330, ARO MURI W911NF-12-1-0461, and NSF-MRSEC DMR-1420541. **Author contributions:** F.S., A.M.C., B.A.B., and T.N. worked out the theoretical results presented here, M.G.V. and Z.W. performed first-principles calculations, and S.S.P.P. contributed the experimental proposal for SnTe nanowires. **Competing interests:** The authors declare that they have no competing interests. **Data and materials availability:** All data needed to evaluate the conclusions in the paper are present in the paper and/or the Supplementary Materials. Additional data related to this paper may be requested from the authors.

Submitted 17 January 2018
Accepted 18 April 2018
Published 1 June 2018
10.1126/sciadv.aat0346

Citation: F. Schindler, A. M. Cook, M. G. Vergniory, Z. Wang, S. S. P. Parkin, B. A. Bernevig, T. Neupert, Higher-order topological insulators. *Sci. Adv.* **4**, eaat0346 (2018).